Behavioral/Systems/Cognitive

Hyperpolarization-Activated Cyclic Nucleotide-Gated Cation Channels Regulate Auditory Coincidence Detection in Nucleus Laminaris of the Chick

Rei Yamada, Hiroshi Kuba, Takahiro M. Ishii, and Harunori Ohmori
Department of Physiology, Faculty of Medicine, Kyoto University, Kyoto 606-8501, Japan

Coincidence detection of bilateral acoustic signals in nucleus laminaris (NL) is the first step in azimuthal sound source localization in birds. Here, we demonstrate graded expression of hyperpolarization-activated cyclic nucleotide-gated (HCN) cation channels along the tonotopic axis of NL and its role in the regulation of coincidence detection. Expression of HCN1 and HCN2, but not HCN3 or HCN4, was detected in NL. Based on measurement of both subtype mRNA and protein, HCN1 varied along the tonotopic axis and was minimal in high-characteristic frequency (CF) neurons. In contrast, HCN2 was evenly distributed. The resting conductance was larger and the steady-state activation curve of I_h was more positive in neurons of middle to low CF than those of high CF, consistent with the predominance of HCN1 channels in these neurons. Application of 8-Br-cAMP or noradrenaline generated a depolarizing shift of the I_h voltage activation curve. This shift was larger in neurons of high CF than in those of middle CF. The shift in the activation voltage of I_h depolarized the resting membrane, accelerated the EPSP time course, and significantly improved the coincidence detection in neurons of high CF, suggesting that I_h may improve the localization of sound sources.

Key words: **hyperpolarization-activated cation channel; coincidence detection; nucleus laminaris; noradrenaline; tonotopy; sound source localization**

Introduction

Sensing interaural time differences (ITDs) is essential for azimuthal sound source localization and requires a neural system that can discriminate extremely small time differences between sound signals detected by two ears. The accuracy of localizing sounds depends on the precision with which ITDs are determined, which in turn depends on the EPSP time course in nucleus laminaris (NL) of birds (Kuba et al., 2003). EPSP time course in NL is affected by two types of ionic currents activated near the resting potential: the dendrotoxin-sensitive low-voltage-activated K^+ current (I_{LK}) and the hyperpolarization-activated cation current (I_h) (Kuba et al., 2003). I_{LK} is activated during membrane depolarization, and its roles in acceleration of EPSP have been reported (Reyes et al., 1996; Kuba et al., 2003, 2005).

I_h is slowly activated during membrane hyperpolarization and is carried by both K^+ and Na^+ (Pape, 1996). Four channel subtypes have been described with different rates of activation and different sensitivities to cyclic nucleotides and are termed hyperpolarization-activated and cyclic nucleotide-gated (HCN) channels (Ludwig et al., 1998, 1999; Santoro et al., 1998; Ishii et al., 1999; Seifert et al., 1999). HCN1 channels are activated faster and at more positive membrane potentials than are HCN2 channels (Santoro and Tibbs, 1999). Conversely, HCN2 channels are more sensitive to intracellular cAMP than are HCN1 channels (Santoro and Tibbs, 1999). The activation kinetics of HCN2 channels are accelerated and the voltage dependence is shifted to the positive direction by the increase of intracellular cAMP. Monoamine and acetylcholine have been shown to modulate I_h by cyclic nucleotide-dependent processes (DiFrancesco et al., 1986; DiFrancesco and Tromba, 1988a,b; Bobker and Williams, 1989). In neurons of the medial nucleus of the trapezoid body (MNTB) in the rat, noradrenaline (NA) has been demonstrated to shift the voltage dependence to a more depolarized potential (Banks et al., 1993); it was suggested that it may be possible to accelerate EPSP and to modulate the capability of MNTB neurons in acoustic signal processing through the activation of I_{LK} by the membrane depolarization caused by I_h.

The precision of coincidence detection in NL depends on the characteristic frequency (CF) of neurons, being the most precise in the middle CF neurons and closely followed by the high CF neurons, and is reduced in the low CF neurons (Kuba et al., 2005). This specialization of middle and high CF neurons as coincidence detectors is likely determined by the robust expression of I_{LK}. Although the conductance of I_h has a tonotopic gradient, it was the highest in the low CF neurons, and apparently I_h has a negative correlation with the precision of coincidence detection (Kuba et al., 2005). Nevertheless, in the present study, we will show the possibility of delicate control of coincidence detection

Received June 21, 2005; revised Aug. 11, 2005; accepted Aug. 14, 2005.

This study was supported by Grant-in-Aid 17023027-0133 from the Ministry of Education (H.O.). We appreciate Dr. L. O. Trussell for careful reading of this manuscript and for valuable comments. We thank Dr. T. Kaneko for kind instruction of preparing the antibody, Dr. R. Shigemoto for a gift of antibody, and Dr. N. Tamamaki for technical advice on *in situ* hybridization. We appreciate M. Fukao for machining the equipment.

Correspondence should be addressed to Harunori Ohmori at the above address. E-mail: ohmori@nbiol.med.kyoto-u.ac.jp.

DOI:10.1523/JNEUROSCI.2541-05.2005

 0270-6474/05/258867-11$15.00/0

by the modulation of gating of HCN channels, paradoxically in the high CF neurons in which the expression of I_h channel was minimal. We will further show that the dominance of HCN2 channels in the high CF neurons is essential for this modulation of coincidence detection.

Materials and Methods

Slice preparation. Animals were kept and used according to the regulations of the Animal Research Committee, Graduate School of Medicine, Kyoto University. Brain slices were cut from chickens (*Gallus domesticus*) of postnatal day 1 (P1) to P7. Detailed procedures of brain slice preparation and maintenance have been published previously (Kuba et al., 2003). During experiments, slices were continuously perfused with normal artificial CSF (ACSF) (in mM: 125 NaCl, 2.5 KCl, 26 $NaHCO_3$, 1.25 NaH_2PO_4, 2 $CaCl_2$, 1 $MgCl_2$, and 17 glucose, pH 7.4). All experiments were performed at 40°C.

Electrophysiological recordings. Whole-cell recordings were made for voltage-clamp experiments with a patch-clamp amplifier (EPC-8; HEKA Elektronik, Lambrecht, Germany) and for current-clamp experiments with a current-clamp amplifier (MEZ-8301; Nihon Kohden, Tokyo, Japan) under an upright microscope (BX50WI; Olympus Optical, Tokyo, Japan) equipped with infrared differential interference contrast optics (C5999; Hamamatsu Photonics, Hamamatsu, Japan). Patch pipettes were fabricated from thin-walled borosilicate glass capillaries (GS150TF-100; Harvard Apparatus, Holliston, MA) and had a resistance of 2–3 MΩ when filled with a KCl-based internal solution (in mM: 160 KCl, 0.2 EGTA, and 10 HEPES-KOH, pH 7.4).

Pipettes were coated with a silicone resin (Sylgard; Dow Corning Asia, Tokyo, Japan), and the tips were fire polished before use. The electrode capacitance was compensated electronically, and the series resistance (3–6 MΩ) was compensated by 60–80%. The liquid junction potential (−3 mV) was corrected after the experiments. $GABA_A$ receptors were blocked by adding 20–40 μM bicuculline (Sigma, St. Louis, MO) in the extracellular medium. In voltage-clamp experiments, recordings were made in ACSF supplemented with 1 mM $BaCl_2$, 1 mM 4-aminopyridine, 1 mM tetraethylammonium-Cl, 200 μM $CdCl_2$, and 1 μM TTX for isolating I_h. When 4-ethylphenylamino-1,2-dimethyl-6-methylaminopyrimidinium chloride (ZD7288) (Tocris Cookson, Ballwin, MO), 8-Br-cAMP (Tocris Cookson), or NA (Sigma) was bath applied, measurements were made at least 5 min after application of the drugs.

Caged cAMP (Calbiochem, Darmstadt, Germany) was used in some experiments. Caged cAMP (20 mM in DMSO stored in darkness at −20°C) was diluted with KCl-based internal solution to the final concentration of 1 mM and was filled in the recording pipette. Photolysis was made by 330–385 nm light from a xenon short-ark lamp (75 W) through a dichroic mirror (400 nm cutoff; U-MWU2; Olympus Optical), by opening the shutter for 1–2 s manually. Spontaneous decomposition of cAMP by trans-illumination was avoided as much as possible by illuminating the preparation through a green interference filter (540–600 nm bandpass and 90% transmission; Nikon, Tokyo, Japan) during the positioning of the electrode.

Electrical stimulation of presynaptic fibers. Biphasic square-wave voltage pulses of 0.1–20 V, 0.1 ms duration were applied through a bipolar tungsten electrode to presynaptic fibers from nucleus magnocellularis (NM). Ipsilateral projection fibers were stimulated by placing the electrode ~50 μm away from the lateral edge of NL. The contralateral projection fibers were stimulated at ~50 μm away from the medial edge of NL.

In experiments to measure synaptic coincidence detection (see Fig. 8*C*,*D*), a pair of stimuli with a 10 ms interstimulus interval was applied, changing the time separation between ipsilateral and contralateral stimuli (Δt). Δt was defined as 0 when the firing probability was maximal and was changed with a step of 0.1 ms between +1 and −1 ms. Positive and negative values indicate contralateral-leading and ipsilateral-leading stimuli, respectively. The firing probability, defined as the total number of spikes divided by the total number of stimuli, was calculated at each Δt from 10 to 30 traces (20–60 stimuli). The time window was determined as the time interval to give the half-maximum firing probability.

Data acquisition and analysis. The CF of neurons was predicted from the mediolateral localization within the nucleus in coronal slices (see Figs. 1*E*, 2*F*), in accordance with previous studies (Rubel and Parks, 1975; Kuba et al., 2005). Current and voltage output signals from the patch-clamp amplifier were filtered at 5 kHz through a four-pole low-pass filter with Bessel characteristics (UF-BL2; NF, Yokohama, Japan) and sampled at 10 kHz by a 12-bit analog-to-digital converter (ADM-8298BPC; Micro Science, Tokyo, Japan) with an in-house data acquisition program. Off-line analysis of data was made using commercially available software (Axograph; Axon Instruments, Union City, CA). In current-clamp experiments, neurons were accepted for analysis if the resting potential was more negative than −58 mV immediately after the whole-cell recording condition was achieved. The input resistance and the membrane time constant were measured from voltage responses to small hyperpolarizing current injection (0.05–0.6 nA). A single-exponential function was used in curve fittings for the high CF and the middle CF neurons; however, a double-exponential function was required for the low CF neurons (Kuba et al., 2005). This could be attributable to a presence of long and thick dendrites in the low CF neurons, and the slower component was adopted as the membrane time constant of the soma (Rall, 1969; Kuba et al., 2005). Data are given as mean ± SEM (n = number of cells). Statistical significance was tested by Student's unpaired t test, unless otherwise stated.

Cloning of chicken HCN1, HCN2, HCN3, and HCN4 and probes for in situ *hybridization.* A single pair of primers for the sequence of rabbit HCN4, containing the S4 to S6 domains (317 bp), was designed: forward, 5′-CAGTGGGAGGAGATCTTCCAC-3′; reverse, 5′-GCAGGTGGCG-CCCACAATC-3′. The longer cDNA clone was obtained by the hybridization of ^{32}P-labeled PCR products with a chicken cDNA library. Sequences of the probe for HCN1 (394 bp), HCN2 (394 bp), HCN3 (400 bp), and HCN4 (394 bp), containing the S1 to S4 domains, were constructed by PCR using the following primer pairs and subcloned in pBluescript (Stratagene, La Jolla, CA): HCN1 forward, 5′-GCGACT-TCAGATTTTACTGGG-3′; HCN1 reverse, 5′-CGTAATAAGCGTAA-CAGGCTG-3′; HCN2 and HCN3 forward, 5′-GCGATTTCAGGTTC-TACTGGG-3′; HCN2 and HCN3 reverse, 5′-CGCAGCAGGC-GCAGCAGGCTG-3′; HCN4 forward, 5′-GCGACTTCAGGTTTTATT-GGG-3′; and HCN4 reverse, 5′-CGCAGGAGCCTCAGGAGGCTG-3′. Digoxigenin (Dig)-labeled RNA probes were synthesized by *in vitro* transcription using the Dig RNA labeling kit (Roche Products, Hertfordshire, UK) following the protocol of the manufacturer.

In situ *hybridization.* Brainstems were dissected from P4–P14 chicks, frozen in a propanol bath embedding medium (Tissue-Tek; Sakura Finetek, Torrance, CA), and sliced coronally on a cryostat at 20 μm. Brain slices were fixed for 10 min in 0.1 M phosphate buffer, pH 7.4, containing 4% paraformaldehyde and washed twice each for 5 min with 0.1 M phosphate buffer. After incubation for 5–10 min at 37°C with 10 μg/ml proteinase K (Roche Products) in 0.1 M Tris, pH 8.0, and 0.05 M EDTA, slices were acetylated with 0.25% acetic anhydride in 0.1 M triethanolamine for 10 min and washed twice each for 5 min with 2× SSC at room temperature. This was followed by prehybridization for 2 h at room temperature in 50% deionized formamide, 5× SSC, 5× Denhardt's solution (Wako, Tokyo, Japan), 250 μg/ml yeast tRNA (Roche Products), and 500 μg/ml salmon sperm DNA (Invitrogen, San Diego, CA). Hybridization was conducted at 60°C for HCN1 mRNA and 65°C for HCN2 mRNA overnight with the denatured Dig-labeled probes in the prehybridization solution (1.25 μg/ml). Slices were then washed three times each for 20 min with 4× SSC, and nondigested probes were degraded by incubation for 30 min at 37°C in RNase solution containing 20 μg/ml RNase A (Sigma), 0.5 M NaCl, 0.01 M Tris, pH 8.0, and 1 mM EDTA. They were then washed with SSC solution with 1 mM dithiothreitol (2× SSC for 5 min, two times each, 1× SSC for 5 min, 0.5× SSC for 5 min, and 0.1× SSC for 30 min at 57°C for HCN1 mRNA and 68°C for HCN2 mRNA, 0.1× SSC for 5 min). Slices were immunoblotted with 1:2000-diluted anti-Dig antibodies conjugated with alkaline phosphatase and were visualized by nitroblue tetrazolium chloride/5-bromo-4-chloro-3-indolyl phosphate salt stock solution (Roche Products). Sense RNA was used as a control, and no significant signals were detected.

Antibodies against chick HCN1 and HCN2. The antibody for rat HCN1, a kind gift from Dr. Shigemoto (National Institute for Physiological Sciences, Okazaki, Japan) (Lörincz et al., 2002), detects the C terminal of rat HCN1 (amino acid residues 850–910). An antibody for chick HCN2 was newly raised. We designed a peptide, CARKDSVGSMPDTDPAKSRLSSNL, which corresponds to the C-terminal 23 amino acids of chick HCN2 protein. N-terminal cysteine was added to couple the peptide with a carrier protein. The peptide was conjugated with maleimide-activated bovine serum albumin (Pierce, Rockford, IL). Guinea pigs were initially immunized by intracutaneous injection of the conjugate (250 μg/animal) in Freund's complete adjuvant (Difco, Detroit, MI) and subsequently boosted by the antigen in incomplete adjuvant after a 4 week interval. The sera were obtained 2 weeks after the boost. The antibody was purified by sodium sulfate fractionation, followed by affinity chromatography on a SulfoLink gel (Pierce) coupled with the peptide (2 mg of peptide per milliliter of gel) and was eluted with 0.1 M glycine-HCl, pH 2.5.

Specificity of HCN1 and HCN2 antibodies was tested with immunoblot analysis of crude membrane fractions prepared from the chick brainstem. Both antibodies gave an immunoreactive band around the molecular mass of 115 kDa for HCN1 and 110 kDa for HCN2 antibody, consistent with previous studies (Ludwig et al., 2003; Notomi and Shigemoto, 2004). HCN2 immunoreactivity disappeared after preadsorption of the antibody with the corresponding synthetic peptide. The adsorption to HCN1 antibody has already been confirmed (Lörincz et al., 2002). These results indicate that the rat HCN1 and affinity-purified HCN2 antibodies specifically recognize chick HCN1 and HCN2 channels.

Immunohistochemistry. After deep anesthesia, six chicks (P6–P8) were perfused transcardially with periodate-lysin-paraformaldehyde fixative (milliliters per gram of body weight): 2% (w/v) paraformaldehyde, 2.7% (w/v) lysin HCl, 0.21% (w/v) $NaIO_4$, and 0.1% (w/v) Na_2HPO_4. The brainstem was dissected out, postfixed for 2 h in medium, and kept overnight in 30% (w/w) sucrose–PBS. Coronal sections (20 μm) were cut with a cryostat and collected in PBS. Sections were incubated overnight at room temperature with 0.63 μg/ml anti-HCN1 antibody or 1 μg/ml anti-HCN2 antibody in PBS containing 0.3% (v/v) Triton X-100, 0.25% (w/v) carrageenan (Nacalai Tesque, Kyoto, Japan), 1% donkey serum, and 0.02% (w/v) sodium azide (PBS-XCD), washed with PBS containing 0.3% (v/v) Triton X-100 (PBS-X), and then incubated for 2 h with 10 μg/ml biotinylated anti-guinea pig IgG donkey antibody (Chemicon, Temecula, CA) in PBS-XCD. After washing with PBS-X, slices were incubated for 1 h with 1 μg/ml Alexa 488-conjugated streptavidin (Molecular Probes, Eugene, OR) in PBS-XCD. The slices were mounted onto glass slides, coverslipped, and observed under a confocal laser-scanning microscope (CSU10; Yokogawa, Tokyo, Japan).

Immunoreactivity of NL neuron was quantitatively measured in two ways by using NIH ImageJ. First, the fluorescence intensity of the dendritic area was measured for three CF regions (see Fig. 2*E*), by setting a circular region of interest of 10–20 μm diameter. Second, the intensity profiles was measured by using the Plot Profile option of NIH ImageJ, along a line drawn crossing the dendritic area from the medial to lateral direction, parallel to the array of NL neurons. The dorsomedial and ventrolateral dendritic areas were measured separately, averaged, and plotted next to each image (see Fig. 2*A*,*B*). In these measurements, the fluorescence intensities of NL neurons were normalized relative to the intensity measured in the medial vestibular nucleus in the same slice. The reference intensities were basically the same across slices ($p > 0.5$; $n = 6$).

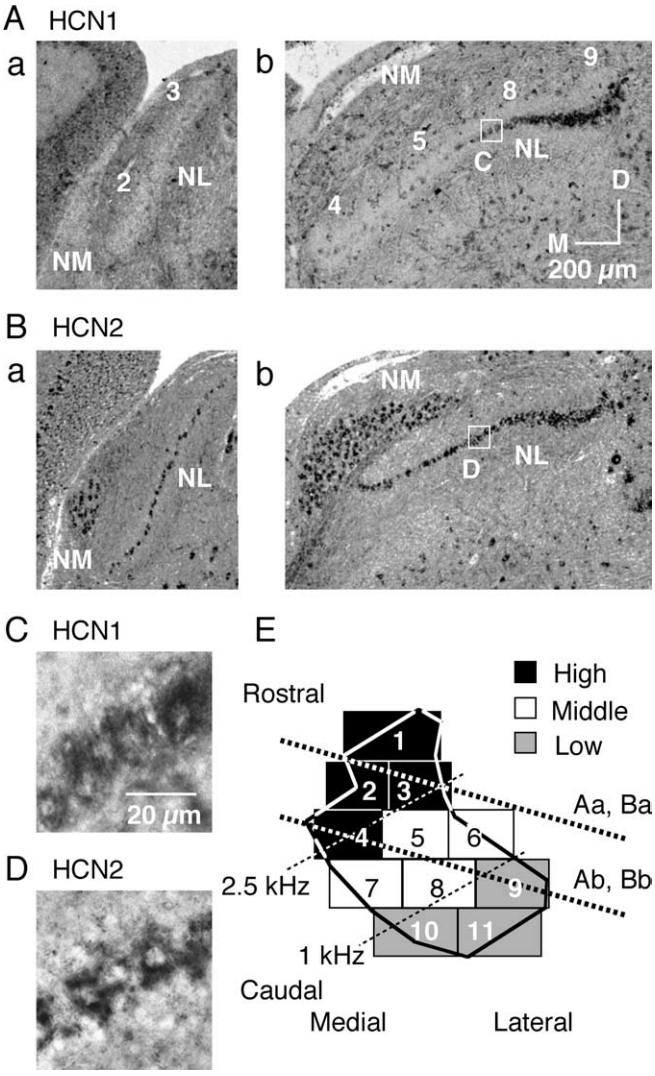

Figure 1. Reduced expression of HCN1 mRNA in the high CF region. ***A***, ***B***, Expression patterns of HCN1 mRNA (***A***) and HCN2 mRNA (***B***), detected by *in situ* hybridization. Orientation of these subcoronal slices is indicated in ***E*** by thick dotted lines. Numbers on each slice (***Aa***, ***Ab***) correspond to sectors indicated in ***E***. M, Medial; D, dorsal. ***C***, ***D***, High magnification of boxes in ***Ab*** and ***Bb***, HCN1 mRNA (***C***) and HCN2 mRNA (***D***). ***E***, Two-dimensional projection of NL (Rubel and Parks, 1975; Kuba et al., 2005). Eleven sectors were defined depending on their rostromedial and caudolateral position within NL and were classified into three CF regions: high (black sectors, 2.5–3.3 kHz), middle (white sectors, 1–2.5 kHz), and low (gray sectors, 0.4–1 kHz).

Results

Tonotopic expression of mRNA of HCN channel subtypes

Following the tonotopic map reported by Rubel and Parks (1975), we divided NL into three CF regions of high, middle, and low as shown in Figure 1*E* (Kuba et al., 2005). By the *in situ* hybridization technique, mRNA expression was detected for HCN1 and HCN2 (Fig. 1*A*,*B*) but not for HCN3 and HCN4 (data not shown). HCN1 expression (Fig. 1*A*) was almost absent in the rostral high CF region (Fig. 1*E*, sectors 2–4, see legend). Expression of HCN1 showed a tendency to increase in the middle CF region (sectors 5, 8) and was high in the low CF region (sector 9); in contrast, HCN2 expression was rather continuous throughout the nucleus (Fig. 1*B*). In the magnified image (Fig. 1*C*,*D*), both HCN1 and HCN2 mRNA were detected in the somatic region, excluding the nuclei, but were practically absent in the neuropil region.

Immunohistochemistry of HCN1 and HCN2

Figure 2 shows the immunoreactivity for HCN1 and HCN2 antibodies in NL neurons. Both HCN1 and HCN2 immunoreactivities were detected in the neuropil region but not in the cell soma (Fig. 2*A*,2*B*; for orientation, see *F*). The absence of immunoreactivity in the cell soma was confirmed by the magnified images of neurons for HCN1 (Fig. 2*C*) and HCN2 (Fig. 2*D*); some immunoreactivity was present surrounding the cell body for HCN2. We are not certain whether the immunoreactivity of HCN2 is on the somatic membrane or on the other components of interven-

ing structures. A stronger immunoreactivity was found in the low CF region for both HCN1 and HCN2 (sectors 9 and 10–11). In the middle CF and high CF regions, expression of HCN2 was not particularly different (Fig. 2*B*); however, HCN1 was reduced in the high CF region (Fig. 2*A*, sectors 2–3, 4). Strong expressions of both channels in the low CF region and the reduced expression of HCN1 in the high CF region are consistent with the observations by *in situ* hybridization (Fig. 1).

We quantified the immunoreactivity of both HCN1 and HCN2 along the tonotopic axis by measuring the immunoreactive fluorescence intensity in the neuropil regions (see Materials and Methods). The intensity profile was plotted in each slice in Figure 2, *A* and *B*, and the average intensity of each CF region in Figure 2*E*. HCN1 immunoreactivity shows a gradual increase toward the low CF region, both in the profile (Fig. 2*A*) and in the average ($p < 0.01$) (Fig. 2*E*). In the intensity profile, HCN2 immunoreactivity was slightly higher in the low CF region (Fig. 2*B*); however, there was no significant difference in HCN2 immunoreactivity among the three CF regions ($p > 0.36$) (Fig. 2*Eb*).

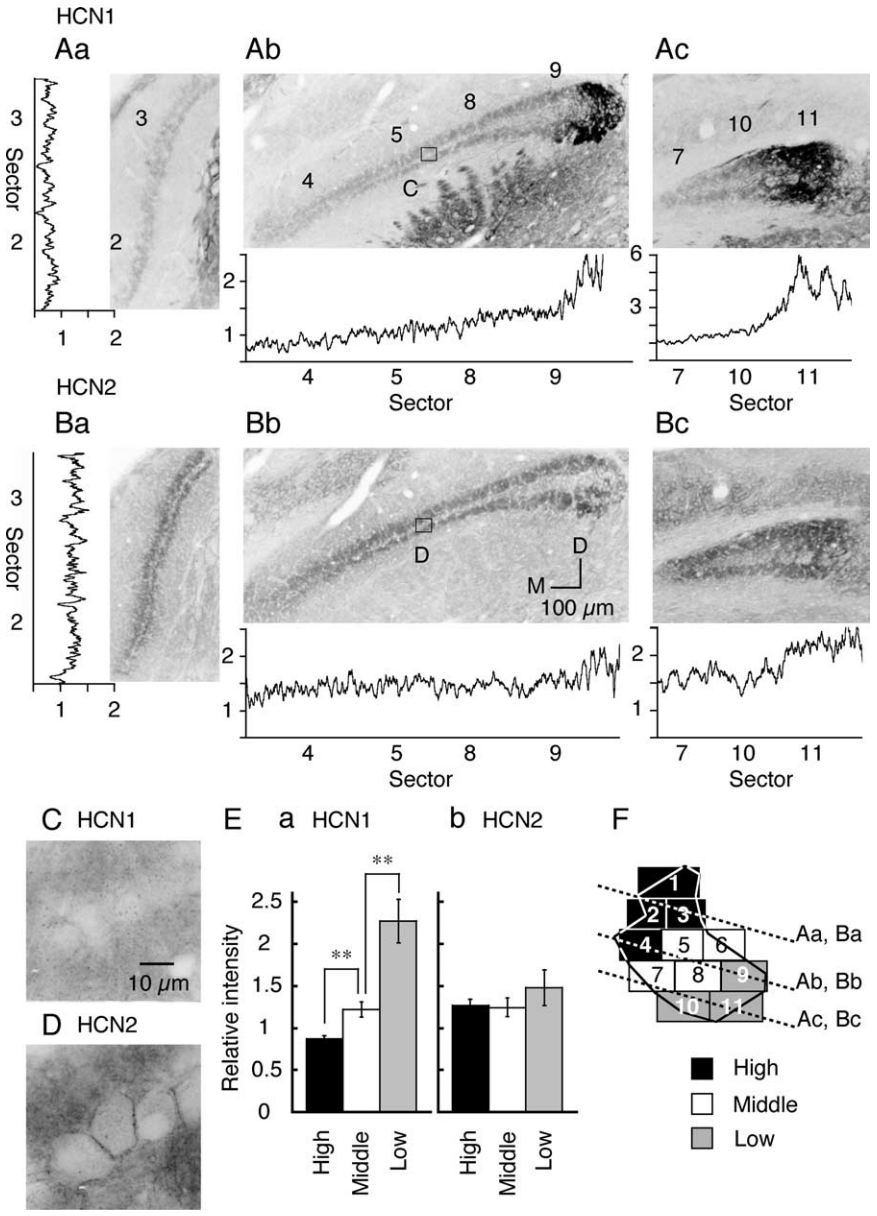

Figure 2. Graded expression of HCN1 channels along tonotopic axis. ***A***, ***B***, Subcoronal slices stained with HCN1 (***A***) and HCN2 (***B***) antibodies. Orientation of these subcoronal slices is indicated in ***F*** by dotted lines. The traces beside each panel are the relative intensity profiles of immunoreactivity in each slice (see Materials and Methods). Numbers on the abscissa indicate the sectors. M, Medial; D, dorsal. ***C***, ***D***, The high magnification of boxes in ***Ab*** and ***Bb***. ***E***, The relative immunoreactivity was measured in the neuropil and averaged for three CF regions (6 chicks). Statistical significance is indicated by $^{**}p < 0.01$ in this and the following figures. ***F***, The relationship of slices to the tonotopic region of the nucleus (see Fig. 1*E*).

Membrane properties around the resting membrane potential

As expected from the immunohistochemical results (Fig. 2), NL neurons have some standing I_h conductance at the resting potential (Kuba et al., 2002b, 2003). After application of ZD7288 (0.1 mM), an organic blocker of I_h channel, the resting potentials of middle CF and low CF neurons were hyperpolarized, although the resting potential was not significantly different among the three CF neurons in the control (Table 1). The responses of cells to current steps were examined in all three CF regions (Fig. 3*A*). When a small constant hyperpolarizing current (−0.6 nA) was injected, the voltage response was the smallest in the middle CF neurons, indicating the lowest input resistance (Fig. 3*D*). All neurons showed a depolarizing voltage sag in response to a large hyperpolarizing current (Fig. 3*A*). This depolarizing sag was absent during bath application of 0.1 mM ZD7288 (Fig. 3*B*), indicating the contribution of I_h. Voltage amplitude was measured at the end of the current step, and the current–voltage (*I–V*) relationship was plotted in Figure 3*C*. The slope conductance was the largest in the middle CF neurons in the control solution, for both the depolarizing and hyperpolarizing directions (Fig. 3*C*, filled circles). Application of ZD7288 made the voltage responses larger and the *I–V* relationships steeper than the controls, particularly in the negative current regions (Fig. 3*C*, open squares).

The input resistance (Fig. 3*D*) and the membrane time constant (Fig. 3*E*) were measured from small voltage responses (smaller than −6 mV) (see Materials and Methods). The CF dependence of time constant and the input resistance was the same as that reported previously (Kuba et al., 2005). Block of I_h by ZD7288 increased both the input resistance and the time constant significantly in the middle CF and the low CF neurons ($p < 0.05$), but the increase was not significant in the high CF neurons ($p > 0.65$) (Fig. 3*D*,*E*). The resting membrane potential was not affected by ZD7288 in the high CF neurons (Table 1). These results indicate that a substantial fraction of the resting conductance was contributed by the resting activation of I_h in the middle CF and the low CF neurons, although not significantly so in the high CF neurons.

EPSP time course

The EPSP was fastest in the middle CF neurons, consistent with the higher resting conductance of this region (Fig. 4*A*, thinner

Table 1. Differences among the three CF neurons with regard to the membrane potential and properties of I_h

	High CF	Middle CF	Low CF
Resting membrane potentials (mV)[a]			
Control[b]	−63.0 ± 0.5 (9)	−62.2 ± 0.5 (29)	−61.6 ± 0.7 (31)
ZD7288 (0.1 mM)	−63.4 ± 0.6 (9)	−64.7 ± 0.9 (12)*	−64.8 ± 0.6 (23)*
Properties of I_h[c]			
Maximum current amplitudes (nA)[d]			
Instantaneous	−0.7 ± 0.1 (15)	−1.8 ± 0.1 (26)	−4.6 ± 0.7 (8)
Steady-state	−2.7 ± 0.2 (15)	−5.2 ± 0.2 (26)	−11.7 ± 1.6 (8)
Activation kinetics (ms)[e]			
τ_{fast}[f]	52.2 ± 3.2 (13)	31.4 ± 1.4 (26)	29.9 ± 3.9 (9)
τ_{slow}[f]	313.3 ± 39.3 (13)	162.8 ± 13.0 (26)	142.7 ± 16.5 (8)
V_h (mV)[f]	−95.5 ± 0.6 (15)	−85.8 ± 0.5 (26)	−85.8 ± 2.8 (8)
S (mV)[b]	9.8 ± 0.3 (15)	10.1 ± 0.3 (26)	9.3 ± 0.3 (8)

Numbers in parentheses are the numbers of cells.

*Statistically significant difference ($p < 0.05$ by unpaired t test) compared with the control in each CF.

[a]Data are from current-clamp experiments (Figs. 3, 4).

[b]Difference was not significant among the three CF neurons ($p > 0.27$).

[c]Data are from voltage-clamp experiments (Fig. 5).

[d]Current amplitude was measured at −143 mV step pulse (Fig. 5). Difference was significant among the three CF regions ($p < 0.01$).

[e]Activation kinetics were measured at −123 mV step pulse (Fig. 5).

[f]Difference was significant between high CF neurons and neurons in the other two regions ($p < 0.01$) but was not significant between middle CF and low CF neurons ($p > 0.1$).

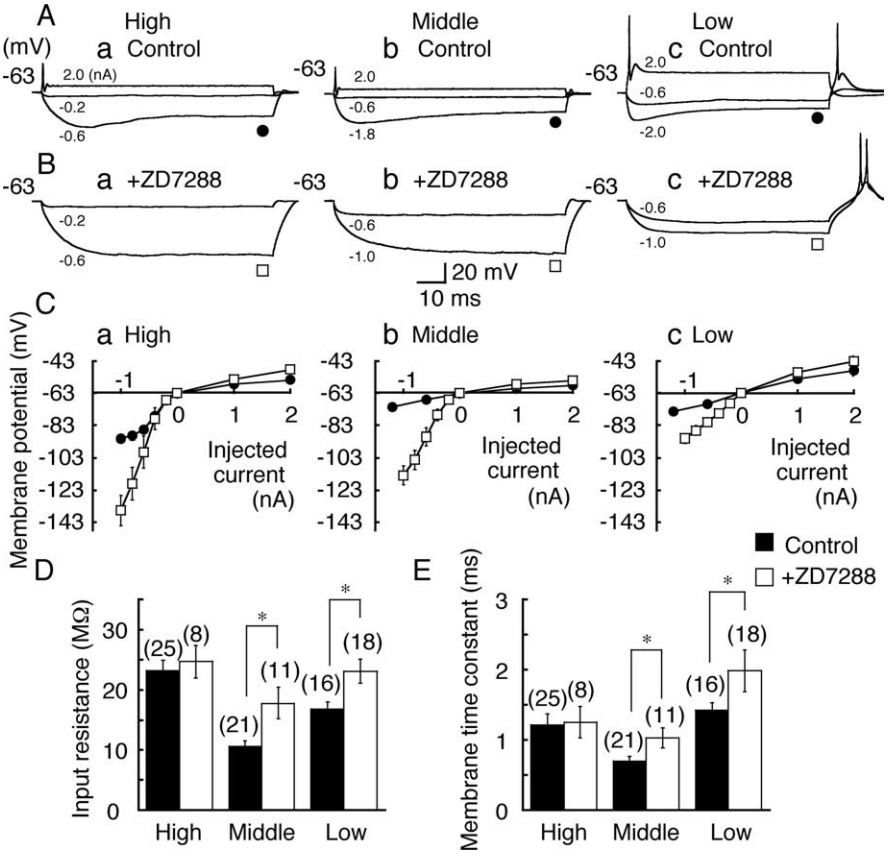

Figure 3. Membrane properties in three CF neurons. ***A***, ***B***, Voltage responses to depolarizing and hyperpolarizing currents of 70 – 80 ms duration in the control (***A***) and after bath application of ZD7288 (0.1 mM) (***B***). For ***A–C***, ***a***, High CF neurons; ***b***, middle CF neurons; ***c***, low CF neurons. The injected currents are indicated in each trace. Holding potential is indicated to the left in this and the following figures. ***C***, Voltage and current relationship measured at the end of current injection of −1.2 to 2 nA in the control (filled circles) and after application of ZD7288 (open squares) was plotted against the injected current (mean ± SE; SE was small and was masked by symbols in the control). ***D***, ***E***, Input resistance (***D***) and membrane time constant (***E***). Filled bars, Control; open bars, in the presence of ZD7288. Numbers in parentheses are the numbers of cells in this and subsequent figures. After application of ZD7288, input resistance and membrane time constant increased significantly in the middle CF and the low CF neurons but not in the high CF neurons. Statistical significance is indicated by *$p < 0.05$ in this and the following figures.

traces) (Kuba et al., 2005). When I_h was blocked by bath application of ZD7288, the time course of EPSP was prolonged in the middle CF and the low CF neurons but was not affected in the high CF neurons ($p > 0.72$) (Fig. 4*A*, thicker traces). The increase of half-amplitude width of EPSP after ZD7288 was significant in the middle CF ($p < 0.01$) and the low CF ($p < 0.05$) neurons (Fig. 4*B*). The 10–90% rise time of EPSP was slightly increased in the low CF neurons ($p < 0.05$) (Fig. 4*C*). Amplitude of EPSP was not affected by ZD7288 (Fig. 4, legend).

I_h among three CF neurons

Properties of I_h were compared among the three CF neurons by voltage-clamp experiments. By the pulse protocols indicated at the bottom of Figure 5*Aa*, membrane potential was changed for 700 ms from −23 to −143 mV at 10 mV intervals to measure the activation of I_h (step 1) and then changed to −143 mV for 300 ms to generate the tail current (step 2). Figure 5*A* illustrates current traces at 20 mV intervals. The hyperpolarizing voltage pulses (step 1) generated inward currents with slow activation kinetics. Amplitude of the inward currents was the smallest and the kinetics of current activation was the slowest in the high CF neurons. The activation kinetics of I_h was examined by fitting the rising phase of step 1 current with an exponential function. The first 5–10 ms was ignored for fitting because of the capacitative transient (Solomon and Nerbonne, 1993). The degree of fit was evaluated by subtracting the fitted curve from the original current trace in Figure 5*B*, for a single (top) and a double (bottom) exponential fitting (currents recorded at −123 mV). Fitting with two exponential functions gave much better results. Figure 5, *Ca* and *Cb*, plots the voltage dependence of two activation time constants. Both the fast and the slow time constants were the largest in the high CF neurons (filled circles) (Table 1). The fraction of the fast component was calculated from the amplitude of the exponential curve fits (Fig. 5*Cc*); the fraction was voltage dependent and increased toward negative potentials, particularly in the high CF neurons. The current–voltage relationships were measured for the current activation for both the instantaneous current and the steady-state current (Fig. 5*E*). The instantaneous current amplitude was measured after the capacitative surge (Fig. 5*D*, diamonds and dashed lines at traces; *E*, dashed lines), the steady-state current at the end of 700 ms voltage pulse (Fig. 5*A*, triangles; *E*, solid lines). The high CF neu-

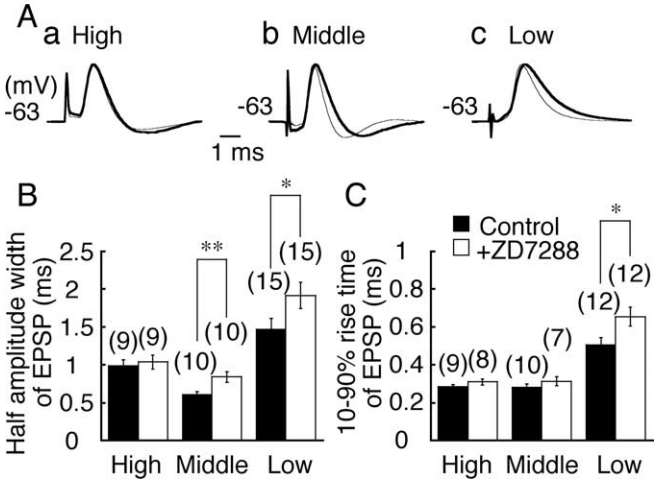

Figure 4. EPSP time course. ***A***, EPSPs recorded before (thinner traces) and after (thicker traces) application of ZD7288 (0.1 mM). ***a***, High CF neuron; ***b***, middle CF neuron; ***c***, low CF neuron. EPSPs were recorded at −63 mV. EPSPs in the control and in ZD7288 were amplitude normalized and superimposed to facilitate comparison of the time course. EPSP amplitude was 6.3 ± 0.8 mV (control) versus 5.8 ± 0.8 mV (ZD7288, $n = 9$; $p = 0.66$) for high CF neurons, 7.8 ± 1.0 versus 6.7 ± 0.7 mV ($n = 10$; $p = 0.38$) for middle CF neurons, and 4.9 ± 0.5 versus 4.4 ± 0.4 mV ($n = 15$; $p = 0.38$) for low CF neurons. ***B***, ***C***, Half-amplitude width (***B***) and 10–90% rise time (***C***) of EPSP in the control (filled bars) and in ZD7288 (open bars).

rons had the smallest slope conductance (filled symbols); thus, the maximum current recorded at −143 mV was the smallest among the three CF regions (Table 1).

Voltage dependence of I_h activation

The voltage dependence of I_h channel activation was estimated from the amplitude of inward tail current generated by a step to −143 mV (step 2) (Fig. 5*A*,*D*). The instantaneous amplitudes of inward tail current (I_{tail}) reflected the conductance activated by preceding step 1 potentials (Fig. 5*D*). When the tail currents were generated from less negative step 1 potentials, the instantaneous current was small and did not change with potentials (Fig. 5*D*, an arrow with a solid line, I_{min}), indicating that the open probability of the channel was nearly zero at these step 1 potentials. When step 1 potentials were more negative, I_{tail} increased (Fig. 5*D*, arrows with a dashed line), and I_{tail} eventually became the same as the maximum current generated at −143 mV (I_{max}, double arrowheads). These indicate that the open probability was increased with the increased negativity of step 1 potential, and the channel was nearly full open when the most negative step 1 potential was applied. The open probability of the I_h channel was, therefore, estimated by plotting the difference of instantaneous tail current amplitude ($I_{tail} - I_{min}$) against step 1 potentials after scaling the maximum difference ($I_{max} - I_{min}$) to 1. The plot is well fitted by the Boltzmann distribution, with a slope factor (S) and a half-amplitude voltage (V_h): $(I_{tail} - I_{min})/(I_{max} - I_{min}) = 1/(1 + \exp((V_m - V_h)/S))$. V_h and S are listed in Table 1. V_m is the membrane potential. S was nearly constant, but V_h was 10 mV more positive in the middle CF and the low CF neurons than in the high CF neurons ($p < 0.01$) (Table 1). This difference reflects the first increase of the tail current amplitude at −93 mV in the high CF neurons, whereas it was at −73 mV in the middle CF and the low CF neurons in Figure 5*D*.

There was a large difference in the magnitude of I_h conductance between the middle CF and the low CF neurons (Fig. 5*E*). However, the activation kinetics and the steady-state open probability were nearly the same (Fig. 5*C*,*F*). This is quite different from the neurons in the high CF region. In addition to the smallest amplitude of I_h, the high CF neurons had the slowest activation kinetics (Fig. 5*C*), and the open probability of I_h was negatively shifted (Fig. 5*F*). This qualitative difference of I_h may account for the absence of effects of ZD7288 on the time course of EPSP in the high CF neurons (Fig. 4). Qualitative differences in I_h may be smaller between the middle CF and the low CF neurons than between the high CF and the other two CF neurons. Therefore, we compared the effects of I_h between the high CF and the middle CF neurons on coincidence detection, in the following study.

Modulation of I_h

The gating of HCN channels is dependent on the intracellular concentration of cAMP, although the dependency is different among family members; HCN2 is more sensitive than HCN1 (Ludwig et al., 1998; Santoro et al., 1998; Santoro and Tibbs, 1999). In MNTB neurons of the rat, incubation by 8-Br-cAMP, a membrane-permeable analog of cAMP, produced a positive shift of the activation curve (Banks et al., 1993). We therefore tested whether the activation of I_h is affected by incubating the slices with 8-Br-cAMP.

Figure 6, *A* and *B*, shows the representative traces before (*a*) and after (*b*) the bath application of 8-Br-cAMP (0.6 mM) in the high CF (*A*) and the middle CF (*B*) neurons. Incubation with 8-Br-cAMP accelerated the activation kinetics of I_h (Fig. 6*C*,*D*) and positively shifted the voltage dependence of I_h activation in neurons from both regions (Fig. 6*E*,*F*). The amplitude of maximum currents was not different: −2.7 ± 0.7 versus −2.6 ± 1.1 nA for the high CF ($p = 0.89$); and −5.2 ± 1.1 versus −4.4 ± 1.3 nA for the middle CF neurons ($p = 0.057$). In the high CF neurons, V_h shifted 10 mV from −95.5 ± 0.6 to −85.4 ± 2.4 mV ($p < 0.01$) (Fig. 6*E*). A limited shift was observed in the middle CF neurons, from −85.8 ± 0.5 to −82.6 ± 1.1 mV ($p < 0.05$) (Fig. 6*F*). The slope factor S was not affected significantly in either neuron ($p > 0.14$). The time constants of activation became smaller in the high CF neurons (Fig. 6*C*), and the fraction of the fast components became less voltage dependent ($p < 0.01$) (Fig. 6*Cc*). In the middle CF neurons, the effects on the time constants were small (Fig. 6*D*). The fractions of the fast and slow components were not affected ($p > 0.09$) (Fig. 6*Dc*). Therefore, the effect of 8-Br-cAMP was greater in the high CF neurons. This seems consistent with the dominance of HCN2 in the high CF region of NL (Figs. 1, 2).

NA modulates I_h

The intracellular concentration of cAMP is regulated through G-protein-coupled mechanisms (Gilman, 1987). NA has been demonstrated to modulate I_h in MNTB neurons of the rat (Banks et al., 1993). Bath application of NA (50 μM) accelerated the activation kinetics of I_h in both high CF and middle CF neurons (Fig. 7*A*,*B*), similar to the effects of 8-Br-cAMP. V_h shifted positively from −95.7 ± 0.6 to −86.4 ± 2.0 mV in the high CF neurons ($p < 0.01$) (Fig. 7*E*) and from −86.7 ± 1.2 to −82.3 ± 1.5 mV in the middle CF neurons ($p < 0.05$) (Fig. 7*F*). S was not affected significantly ($p > 0.14$). Two time constants of activation were slightly shortened in the high CF neurons ($p < 0.05$) (Fig. 7*C*) but were not different in the middle CF neurons ($p > 0.13$) (Fig. 7*D*). The fraction of fast and slow kinetics component was not affected in either neuron ($p > 0.08$).

NA depolarizes high CF neurons

The resting membrane potential in the high CF neurons was depolarized by incubation with NA to −59.9 ± 0.8 mV from the

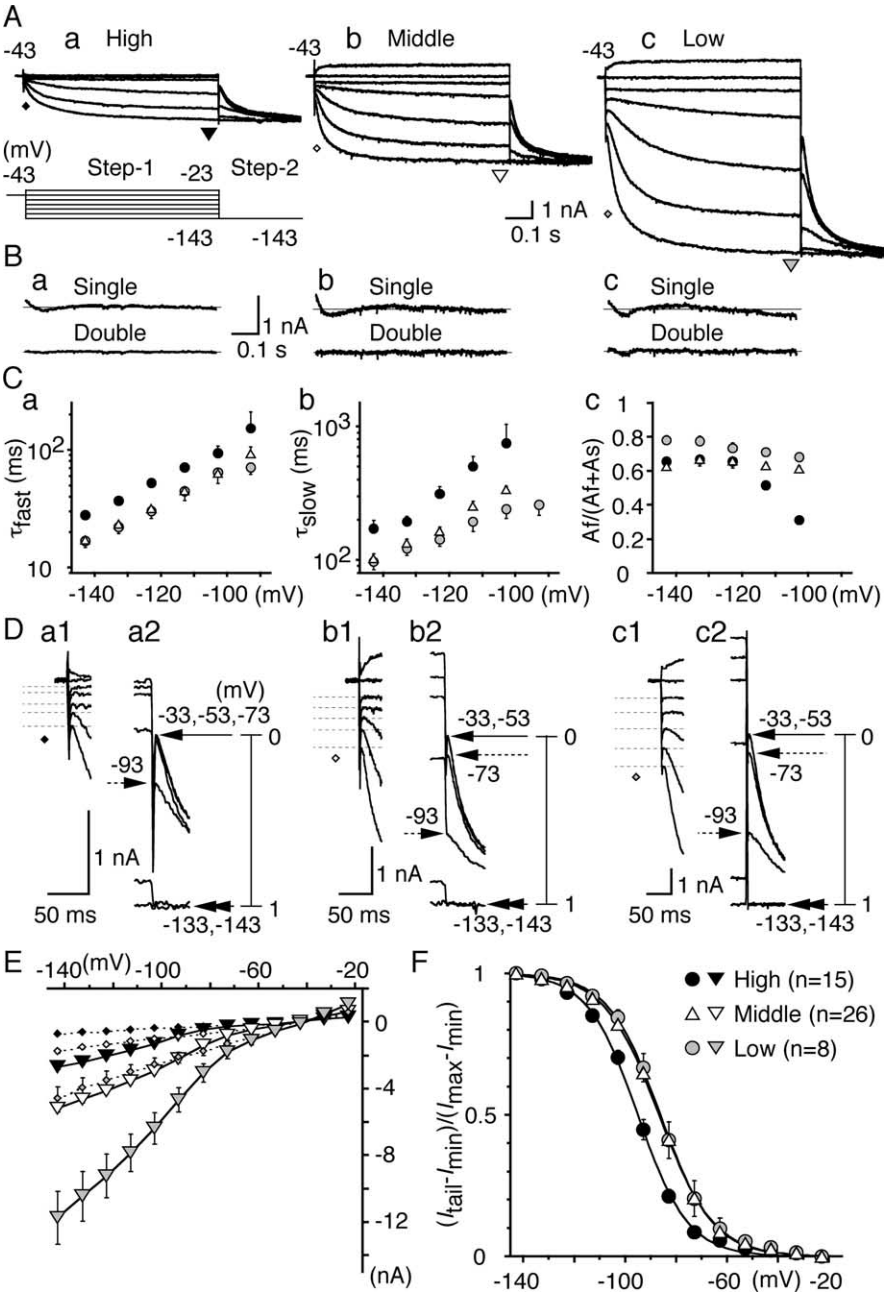

Figure 5. Comparison of I_h among three CF neurons. ***A***, Representative current traces. For ***A***, ***B***, and ***D***, ***a***, High CF neurons; ***b***, middle CF neurons; ***c***, low CF neurons. The pulse protocol is indicated at the bottom of ***Aa***. The same pulse protocol was used in subsequent voltage-clamp experiments (Figs. 6, 7). The initial current and the steady-state current were measured at the times indicated by diamonds (see also ***D***) and triangles. ***B***, Difference between the data and the curve fits for the single (top) and double (bottom) exponential functions (see Results). The double-exponential fit gave much better results than the single-exponential fit. ***C***, Fast (***a***) and slow (***b***) time constants of current activation and the fraction of fast component (***c***) were plotted against step 1 potential. For ***C***, ***E***, and ***F***, Black symbols, High CF neurons; white symbols, middle CF neurons; gray symbols, low CF neurons. ***D***, The expanded traces after step 1 (***a1***, ***b1***, ***c1***) and step 2 (***a2***, ***b2***, ***c2***). Amplitude of initial current was measured at the peak, indicated by dashed lines (***a1***, ***b1***, ***c1***), and averaged value was plotted in ***E*** (diamonds). Tail current amplitude ($I_{tail} - I_{min}$) was scaled between 0 and 1 and was plotted against the step 1 potential in ***F***. Step 1 potentials are indicated at corresponding tail currents. ***E***, *I–V* relationships of both initial (diamonds) and steady-state (inverted triangles) current measured at the times indicated in ***A*** and ***D***. SEs were small and were masked by the symbols in the high CF and the middle CF neurons. ***F***, Voltage dependence of activation measured from the tail current. Solid lines are the Boltzmann fits to the average data. V_h and *S* (see Results) were measured in each experiment and averaged (Table 1). Note that the voltage dependence was 10 mV more positive in the middle CF and low CF neurons than that in the high CF neurons ($p < 0.01$).

original resting potential of −64.5 ± 0.7 mV ($n = 11$; paired *t* test, $p < 0.01$) (Fig. 8*A*). In the middle CF neurons, the resting potential was not significantly affected: from −63.4 ± 0.7 to −61.9 ± 0.2 mV ($n = 4$; paired *t* test, $p = 0.08$) (Fig. 8*B*). The depolarization induced by NA in the high CF neurons was accompanied by a decrease in input resistance from 23.9 ± 3.9 to 15.5 ± 2.8 MΩ ($n = 11$; $p < 0.01$). In the presence of ZD7288, high CF neurons were not depolarized by NA, indicating that the membrane depolarization was induced by I_h; the resting potential was −62.5 ± 0.8 mV in ZD7288 and was −62.1 ± 0.9 mV after application of NA in ZD7288 ($n = 5$; $p = 0.14$).

NA and photolysis of caged cAMP accelerate the EPSP time course in the high CF neurons

A nearly 10 mV positive shift of I_h activation along the voltage axis (Fig. 7*E*) and 5 mV positive shift of resting potential (Fig. 8*A*) by NA might affect the time course of EPSP. After NA, the EPSP time course was accelerated and the EPSP amplitude was reduced significantly in the high CF neurons, but neither occurred in the middle CF neurons (Fig. 8*A*,*B*). The half-amplitude width of EPSP was 1.28 ± 0.08 ms in the control versus 0.92 ± 0.04 ms in NA in high CF ($n = 11$; $p < 0.01$) and 0.80 ± 0.09 versus 0.77 ± 0.07 ms ($n = 4$; $p = 0.66$) in middle CF neurons. The amplitude of EPSP was 6.8 ± 0.6 versus 5.5 ± 0.6 mV in high CF ($n = 11$; $p < 0.01$) and 6.5 ± 0.7 versus 6.3 ± 0.8 mV ($n = 4$; $p = 0.66$) in middle CF neurons. The 10–90% rise time of EPSP was not affected significantly in either neuron ($p > 0.24$). Caged cAMP (1 mM) was introduced to cells through the recording patch pipette. When the intracellular cAMP concentration was elevated by photolysis in the high CF neurons, the membrane potential was depolarized from −63.3 ± 1.4 to −61.1 ± 1.4 mV ($n = 7$; paired *t* test, $p < 0.01$), the input resistance was decreased from 21.5 ± 1.6 to 16.2 ± 1.5 MΩ ($p < 0.01$), and the EPSP time course was accelerated; the half-amplitude width of EPSP was decreased from 1.22 ± 0.06 to 1.00 ± 0.05 ms ($p < 0.01$). The amplitude of EPSP was not affected ($p = 0.47$). The changes of the input resistance (0.75-fold) and the half-amplitude width of EPSP (0.82-fold) were not statistically different from the changes observed after incubation with NA ($p = 0.17$). In the middle CF neurons, neither the resting membrane potential nor the EPSP time course was affected significantly by photolysis of caged cAMP ($p > 0.06$; $n = 6$).

Effects of membrane depolarization by current injection on the EPSP

Application of NA and photolysis of caged cAMP activated I_h and depolarized the membrane. When the membrane potential was

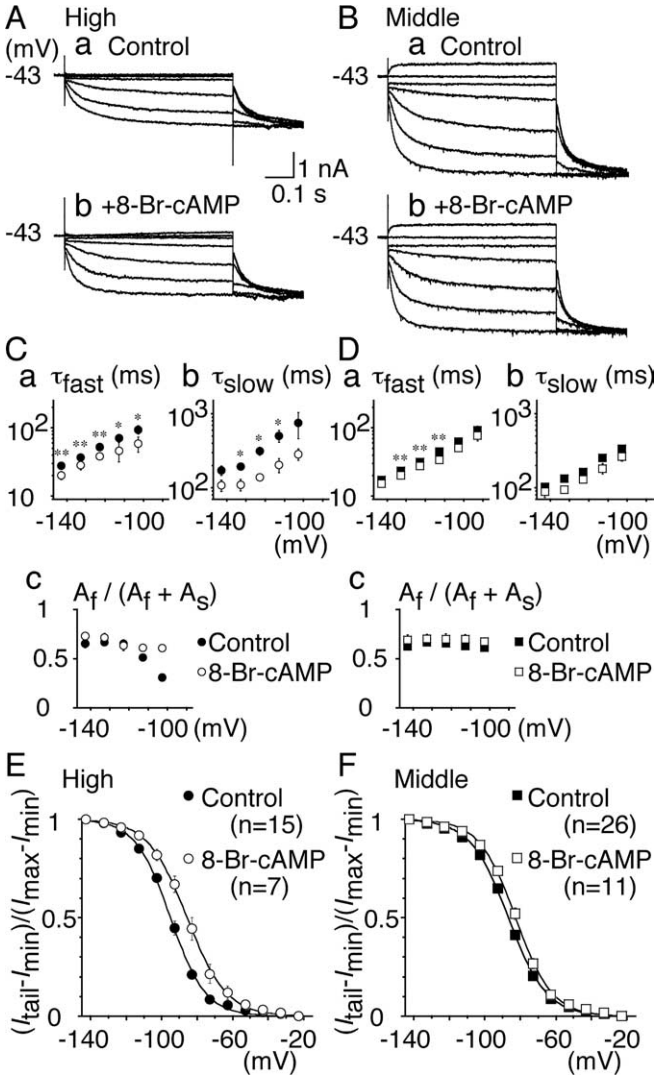

Figure 6. Modulation of I_h by 8-Br-cAMP. ***A***, ***B***, Representative current traces recorded before (***a***) and after (***b***) bath application of 8-Br-cAMP (0.6 mM). Recordings were made in the same cells. ***A***, High CF neurons; ***B***, middle CF neurons. ***C***, ***D***, Fast (***a***) and slow (***b***) time constants and the fraction of the fast component (***c***) were plotted. For ***C–F***, Filled symbols, Control; open symbols, 8-Br-cAMP. ***C***, High CF neurons; ***D***, middle CF neurons. In the middle CF neurons, the fast time constant was slightly shortened, but the slow time constant was not affected ($p > 0.07$). ***E***, ***F***, Voltage-dependent activation curves. In high CF neurons (***E***), $V_h = -95.5$ and $S = 9.8$ mV for control; $V_h = -85.4$ and $S = 10.6$ mV in 8-Br-cAMP ($p < 0.01$). In middle CF neurons (***F***), $V_h = -85.8$ and $S = 10.1$ mV for control; $V_h = -82.6$ and $S = 10.0$ mV in 8-Br-cAMP ($p < 0.05$).

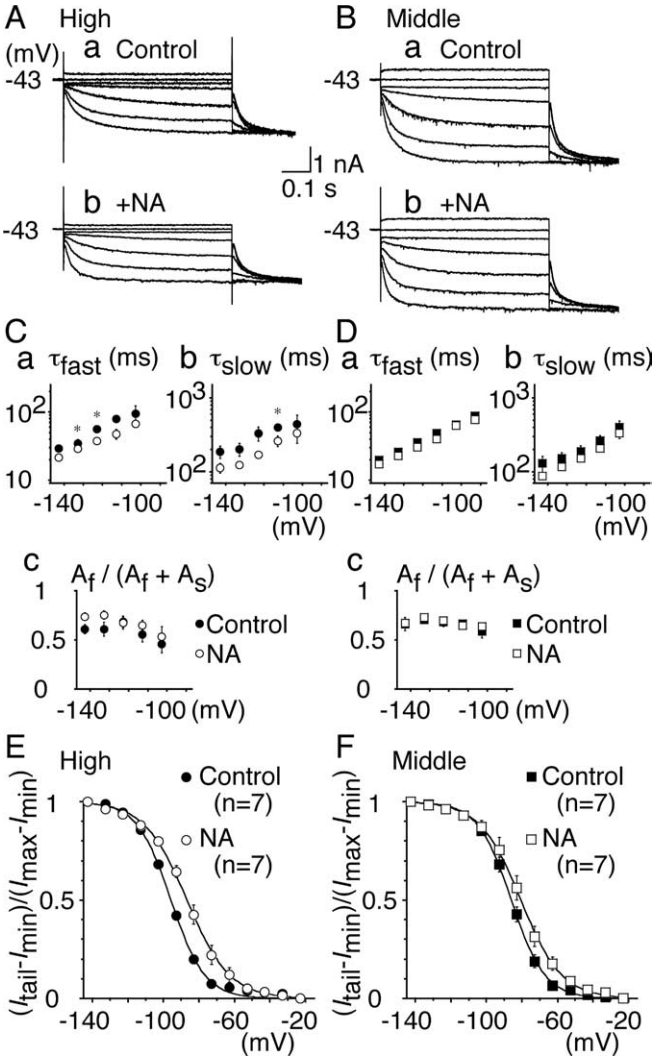

Figure 7. Modulation of I_h by NA. ***A***, ***B***, Representative current traces recorded before (***a***) and after (***b***) bath application of NA (50 μM). Recordings were made in the same cells. ***A***, High CF neurons; ***B***, middle CF neurons. ***C***, ***D***, Fast (***a***) and slow (***b***) time constants and the fraction of the fast component (***c***) were plotted. For ***C–F***, Filled symbols, Control; open symbols, NA. ***C***, High CF neurons; ***D***, middle CF neurons. ***E***, ***F***, Voltage dependence of activation curves. In high CF neurons (***E***), $V_h = -95.7$ and $S = 9.8$ mV for control; $V_h = -86.4$ and $S = 11.7$ mV in NA ($p < 0.01$). In middle CF neurons (***F***), $V_h = -86.7$ and $S = 9.9$ mV for control; $V_h = -82.3$ and $S = 10.4$ mV in NA ($p < 0.05$). Note that NA mimicked the effects of 8-Br-cAMP.

depolarized by 5 mV without activating I_h but by current injection in the high CF neurons, equivalent to the depolarization induced by NA incubation or by photolysis of caged cAMP, the following occurred: the input resistance was decreased from 26.7 ± 7.9 to 17.9 ± 5.9 MΩ ($n = 11$; paired t test, $p < 0.01$), the half-amplitude width of EPSP was accelerated from 1.05 ± 0.06 to 0.77 ± 0.04 ms ($p < 0.01$), and the amplitude of EPSP was decreased from 4.8 ± 0.3 to 4.1 ± 0.2 mV ($p < 0.05$). The extent of decrease of the half-amplitude width and the amplitude of EPSP were 0.74-fold and 0.89-fold, respectively. These changes were almost the same as those attributable to the effect of NA ($p > 0.3$) and attributable to the photolysis of caged cAMP ($p > 0.2$). Therefore, it is most likely that NA accelerates the EPSP through the depolarization induced by the shift of activation of HCN2 channels (Fig. 7*E*).

When NA was applied to the high CF neuron while holding the membrane potential at the resting level (−64.6 ± 0.8 mV; $n = 4$) by current injection, the shape of EPSP was not affected; the half-amplitude width of EPSP was 1.08 ± 0.13 versus 0.97 ± 0.06 ms ($p = 0.32$), and the amplitude of EPSP was 5.0 ± 0.8 versus 4.5 ± 0.9 mV ($p = 0.15$), respectively, in the control and in NA.

NA improved the precision of coincidence detection in the high CF neurons

The coincidence detection in NL was the most precise in the middle CF neurons (time window of 0.31 ms), closely followed by the high CF neurons (0.54 ms), and was the worst in the low CF neurons (1.35 ms) (Kuba et al., 2005). Because the time course of EPSP is accelerated in the high CF neurons by incubation with NA (Fig. 8*A*), this might affect the precision of coincidence detection in the high CF neurons. The precision of coincidence detection has a positive correlation with the time course of EPSP

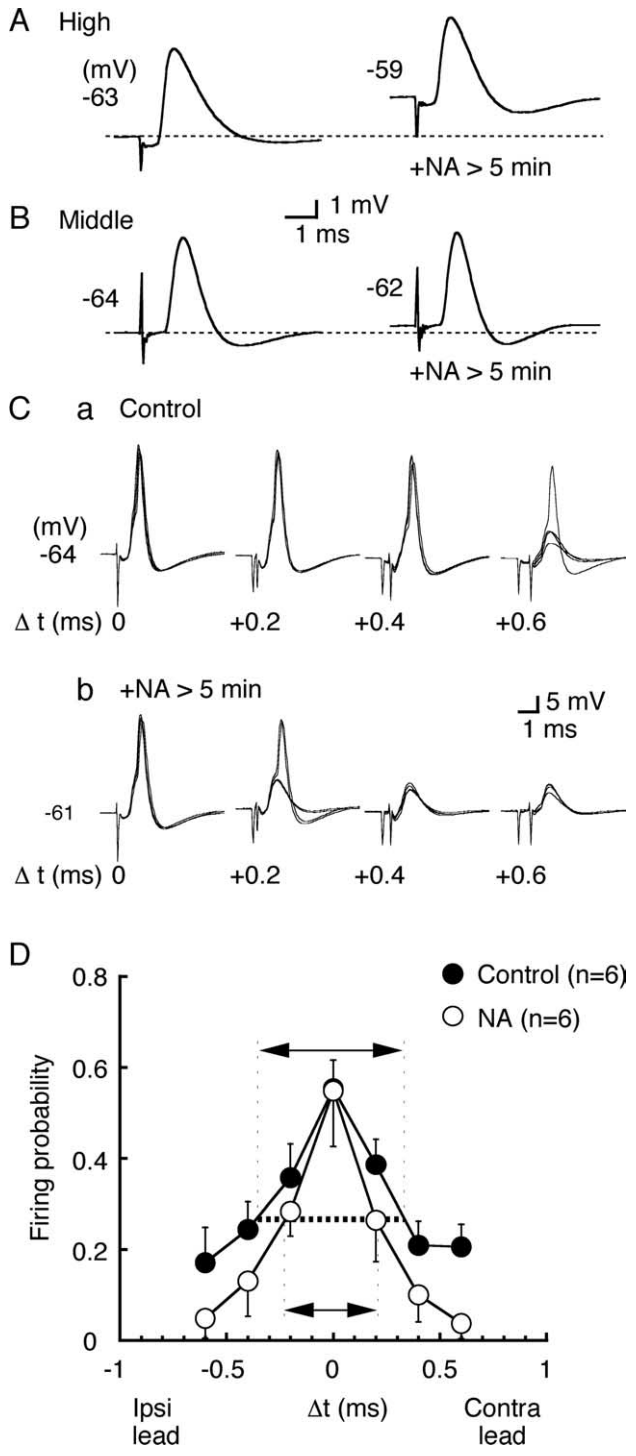

Figure 8. NA accelerates EPSP and improves the coincidence detection in high CF neurons. ***A***, ***B***, EPSPs were recorded before and after bath application of NA (50 μM) in the same cells. ***A***, High CF neurons; ***B***, middle CF neurons. The membrane potential is indicated near the trace, and the dashed line indicates the level of resting membrane potential. ***C***, Four superimposed voltage traces in response to bilateral stimuli at different stimulus time intervals (Δt in milliseconds, indicated in the figure). ***a***, Before bath application of NA; ***b***, after bath application of NA. ***D***, Probability of spike generation as a function of Δt was calculated from six neurons. Note that the time window (arrows) was reduced after application of NA ($p < 0.05$).

(Funabiki et al., 1998; Kuba et al., 2003), and smaller amplitude of the EPSP is also known to improve the coincidence detection (Kuba et al., 2002a; Cook et al., 2003). In Figure 8*C*, the coincidence detection was tested in the high CF neurons by changing the time interval (Δt) between two electrical stimuli applied to the projection from the ipsilateral NM and from the contralateral NM. Figure 8*D* plots the average firing probability against the stimulus time interval (Δt), and the precision of coincidence detection was evaluated as the time window to give the half-maximum firing probabilities (indicated by arrows). We examined six cells in the high CF region, and application of NA caused the improvement of coincidence detection in all six neurons. Mean time window was 0.70 ± 0.12 ms in the control and 0.43 ± 0.08 ms after application of NA, and this difference was statistically significant ($p < 0.05$). The mean resting potential was depolarized from −64.7 ± 0.3 to −61.5 ± 0.8 mV, the mean half-amplitude width of EPSP was reduced from 1.10 ± 0.13 to 0.88 ± 0.05 ms, and the mean amplitude of EPSP was reduced from 7.9 ± 0.6 to 6.4 ± 0.7 mV ($p < 0.01$). EPSP was measured from traces when action potential failed.

NA application depolarized the resting potential and affected the threshold and the rate of rise of action potentials; the threshold potential was positively shifted from −51.6 ± 0.5 to −49.8 ± 0.9 mV ($p < 0.05$), and the maximum rate of rise was reduced from 112.2 ± 11.8 to 90.3 ± 12.4 V/s ($p < 0.01$). This may be reflected in the reduced firing probability at the out-of-coincident timings, whereas the probability of firing was not different when stimulus was applied in coincidence (Fig. 8*D*).

When the resting membrane was depolarized by 5 mV by current injection, it reduced the time window of coincidence detection from 0.91 ± 0.13 to 0.51 ± 0.16 ms ($n = 4$; paired t test, $p < 0.05$). The maximum rate of rise of action potential was reduced 0.84-fold ($p < 0.01$), and the threshold potential was positively shifted by 2.6 ± 0.1 mV ($p < 0.01$). These changes were almost the same as the changes induced by NA ($p > 0.32$). Therefore, NA probably improved the precision of coincidence detection solely by the depolarization it induced.

Discussion

We have shown that the distribution of HCN channels and the properties of I_h are different along the tonotopic axis (Figs. 1, 2, 5). I_h contributed significantly to the input resistance of neurons (Fig. 3*D*), and the time course of EPSP was accelerated by the presence of I_h in the middle CF and the low CF neurons (Fig. 4). I_h was least expressed in the high CF neurons; however, the modulation of gating kinetics by NA and 8-Br-cAMP was most obvious in the high CF neurons (Figs. 6, 7) because of the dominance of HCN2 channels. Consequently, the precision of coincidence detection was improved by the membrane depolarization induced by NA incubation in the high CF neurons (Fig. 8*D*).

HCN subtypes

In NL, both HCN1 and HCN2 channels were expressed throughout the nucleus. The expression of HCN2 channels was relatively uniform, but that of HCN1 channels showed a gradient of increase from the high CF to the low CF neurons (Figs. 1, 2). HCN1 channels have faster activation kinetics and a more positive voltage dependence of activation than HCN2 channels do (Santoro and Tibbs, 1999; Santoro et al., 2000; Moosmang et al., 2001). The slower activation kinetics and more negative voltage dependence of I_h in the high CF neurons (Fig. 5) are consistent with the reduced expression level of HCN1 channels there. Between the middle CF and the low CF neurons, the properties of I_h were not significantly different with regard to the kinetics and the voltage dependence of activation, with the only difference being found in the absolute level of conductance (Table 1).

I_h depolarizes the middle CF and low CF neurons

The extent of resting activation of I_h was CF dependent. Approximately 15% of I_h was activated in the middle CF and the low CF neurons, whereas <5% was activated in the high CF neurons (Fig. 5). This resting activation of I_h conductance contributed to the time course of EPSP in the middle CF and low CF neurons (Fig. 4). The resting membrane potential did not vary along the tonotopic axis (Table 1), and the block of I_h by ZD7288 hyperpolarized the resting membrane of the middle CF neurons by 2.5 mV and the low CF neurons by 3.2 mV; the high CF neurons were not affected (Table 1). This is because I_h conductance acts as a shunting conductance and depolarizes the membrane slightly; the reversal potential of I_h is approximately −50 to −20 mV (Pape, 1996; Santoro and Tibbs; 1999; Robinson and Siegelbaum, 2003).

ZD7288 is known as a specific organic blocker of I_h, but some other effects of the compound have been reported recently in relation to synaptic transmission (Chevaleyre and Castillo, 2002; Chen, 2004). After application of ZD7288 in the middle CF and low CF neurons, a prolongation of EPSP time course was observed (Fig. 4), but those were the same as observed previously by applying Cs^+ to block I_h (Kuba et al., 2003), and amplitude of EPSP was not affected by ZD7288 either ($p > 0.38$); thus, effects of ZD7288 on synaptic transmission might be negligible in NL.

NA depolarized the resting membrane, accelerated the EPSP, and improved the coincidence detection in the high CF neurons

The coincidence detection is very precise in NL, with the best precision in the middle CF neurons and only slightly lower in the high CF neurons (Kuba et al., 2005). We observed that NA can improve the coincidence detection in the high CF neurons (Fig. 8*D*). This suggests the possibility of neuronal modulation of coincidence detection during auditory sound source localization. In the high CF neurons, application of 8-Br-cAMP and NA positively shifted the activation of I_h by 10 mV (Figs. 6*E*, 7*E*). This corresponds to the increase of the fraction of channel activation, from <5 to ~13% at the resting membrane potential (Fig. 6*E*, 7*E*), and likely leads to depolarization of approximately +5 mV in the high CF neurons (Fig. 8*A*). This membrane depolarization accelerated the EPSP time course and reduced the amplitude of EPSP. Also, the depolarization generated by current injection demonstrated almost the same effects on EPSP as NA did. In the test of coincidence detection by membrane depolarization induced by both NA and current injection, the firing probability was not different when bilateral stimuli were applied in coincidence. However, it was reduced significantly when stimuli were applied out of coincidence, thereby making the profile of the coincidence detection curve steeper (Fig. 8*D*). It is known that both the time course of EPSP (Funabiki et al., 1998; Kuba et al., 2003) and the amplitude of EPSP (Kuba et al., 2002a; Cook et al., 2003) affect the precision of coincidence detection. Thus, reducing the width and the amplitude of EPSP would lead to the improvement of coincidence detection, and these effects are likely attributable to the increased activation of I_{LK} by depolarization of the membrane (Rathouz and Trussell, 1998). The membrane depolarization also reduced the maximum rate of rise of action potential and increased the firing threshold. These effects might have reduced the probability of action potential generation at noncoincidence stimuli. The partial inactivation of the sodium channel conductance during depolarization could also improve the coincidence detection (Reyes et al., 1996).

In the middle CF neurons, which have a more extensive expression of HCN1 channel than the high CF neurons, application of NA shifted the voltage dependence of I_h activation by 3 mV. This might have been too small to be reflected in the improvement of coincidence detection.

Sources of noradrenaline

Some modulatory effects of NA were demonstrated on neurons in the mammalian auditory system (Kössl and Vater, 1989; Banks et al., 1993). Iontophoretic application of NA enhances the auditory temporal contrast and improves the precision of neuronal timing coding in bushy cells of the anteroventral cochlear nucleus (Kössl and Vater, 1989). NA shifted the voltage dependence of I_h to a more depolarized potential in MNTB neurons (Banks et al., 1993). Immunohistochemical studies have shown that NA is present in nerve endings within the superior olivary complex (Wynne and Robertson, 1996). Superior olivary complex is part of the ascending auditory pathway and consists of several subnuclei, including the medial superior olive, a mammalian homolog of NL. The noradrenergic input to superior olivary complex originates solely from the nucleus locus ceruleus (Mulders and Robertson, 2001). Neurons in nucleus locus ceruleus have been shown to increase their activity during a high level of arousal (Aston-Jones and Bloom, 1981). Although details of projections from nucleus locus ceruleus are not known in the chicken, noradrenergic fibers are demonstrated in numerous part of the brainstem, including NL (Moons et al., 1995).

Physiological effects of I_h for the localization of sound source

Among chick NL neurons, the middle CF neurons have the large I_{LK} and I_h conductance, thus accelerating their EPSP time course and making the coincidence detection sharpest (Kuba et al., 2005). The high CF neurons had the precision of coincidence detection slightly lower than the middle CF neurons (Kuba et al., 2005). Although the I_h conductance was the smallest, the findings in this paper suggest that the high CF neurons might increase the precision of coincidence detection *in vivo* by NA through the modulation of I_h gating. In contrast, the low CF neurons have the largest I_h conductance, but the precision of coincidence detection is the lowest (Kuba et al., 2005). In the low CF neurons, dendrites are thick and extremely long (Smith and Rubel, 1979; Kuba et al., 2005), suggesting a possibility that I_h may be involved in signal processing at dendrites (Magee, 1998); however, the roles of the large I_h conductance in the low CF neurons remain to be investigated.

ITDs are calculated separately at each CF at NL. After convergence of frequency channels in the higher-order neurons, ITD discrimination seems improved (Konishi, 2003). Behaviorally, the error of sound source localization is known to be reduced when stimulated by a broadband noise in the owl (Knudsen and Konishi, 1979), and the resolution for detecting ITD increases with stimulus bandwidth in human (Klumpp and Eady, 1956). Therefore, the modulation of I_h by NA during a high level of arousal (Aston-Jones and Bloom, 1981) might improve the resolution of sound source localization.

References

Aston-Jones G, Bloom FE (1981) Activity of norepinephrine-containing locus coeruleus neurons in behaving rats anticipates fluctuations in the sleep-waking cycle. J Neurosci 1:876–886.

Banks MI, Pearce RA, Smith PH (1993) Hyperpolarization-activated cation current (I_h) in neurons of the medial nucleus of the trapezoid body: voltage-clamp analysis and enhancement by norepinephrine and cAMP suggest a modulatory mechanism in the auditory brain stem. J Neurophysiol 70:1420–1432.

Bobker DH, Williams JT (1989) Serotonin augments the cationic current I_h in central neurons. Neuron 2:1535–1540.

Chen C (2004) ZD7288 inhibits postsynaptic glutamate receptor-mediated responses at hippocampal perforant path-granule cell synapses. Eur J Neurosci 19:643–649.

Chevaleyre V, Castillo PE (2002) Assessing the role of Ih channels in synaptic transmission and mossy fiber LTP. Proc Natl Acad Sci USA 99:9538–9543.

Cook DL, Schwindt PC, Grande LA, Spain WJ (2003) Synaptic depression in the localization of sound. Nature 421:66–70.

DiFrancesco D, Tromba C (1988a) Inhibition of the hyperpolarization-activated current (i_f) induced by acetylcholine in rabbit sino-atrial node myocytes. J Physiol (Lond) 405:477–491.

DiFrancesco D, Tromba C (1988b) Muscarinic control of the hyperpolarization-activated current (i_f) in rabbit sino-atrial node myocytes. J Physiol (Lond) 405:493–510.

DiFrancesco D, Ferroni A, Mazzanti M, Tromba C (1986) Properties of the hyperpolarizing-activated current (i_f) in cells isolated from the rabbit sino-atrial node. J Physiol (Lond) 377:61–88.

Funabiki K, Koyano K, Ohmori H (1998) The role of GABAergic inputs for coincidence detection in the neurones of nucleus laminaris of the chick. J Physiol (Lond) 508:851–869.

Gilman AG (1987) G proteins: transducers of receptor-generated signals. Annu Rev Biochem 56:615–649.

Ishii TM, Takano M, Xie LH, Noma A, Ohmori H (1999) Molecular characterization of the hyperpolarization-activated cation channel in rabbit heart sinoatrial node. J Biol Chem 274:12835–12839.

Klumpp RG, Eady HR (1956) Some measurements of interaural time difference thresholds. J Acoust Soc Am 28:859–860.

Knudsen EI, Konishi M (1979) Mechanisms of sound localization in the barn owl (*Tyto alba*). J Comp Physiol A Neuroethol Sens Neural Behav 133:13–21.

Konishi M (2003) Coding of auditory space. Annu Rev Neurosci 26:31–55.

Kössl M, Vater M (1989) Noradrenaline enhances temporal auditory contrast and neuronal timing precision in the cochlear nucleus of the mustached bat. J Neurosci 9:4169–4178.

Kuba H, Koyano K, Ohmori H (2002a) Synaptic depression improves the coincidence detection at nucleus laminaris in brainstem slices of the chick embryo. Eur J Neurosci 15:984–990.

Kuba H, Koyano K, Ohmori H (2002b) Development of membrane conductance improves coincidence detection in the nucleus laminaris of the chicken. J Physiol (Lond) 540:529–542.

Kuba H, Yamada R, Ohmori H (2003) Evaluation of the limiting acuity of coincidence detection in nucleus laminaris of the chicken. J Physiol (Lond) 552:611–620.

Kuba H, Yamada R, Fukui I, Ohmori H (2005) Tonotopic specialization of auditory coincidence detection in nucleus laminaris of the chick. J Neurosci 25:1924–1934.

Lörincz A, Notomi T, Tamas G, Shigemoto R, Nusser Z (2002) Polarized and compartment-dependent distribution of HCN1 in pyramidal cell dendrites. Nat Neurosci 5:1185–1193.

Ludwig A, Zong X, Jeglitsch M, Hofmann F, Biel M (1998) A family of hyperpolarization-activated mammalian cation channels. Nature 393:587–591.

Ludwig A, Zong X, Stieber J, Hullin R, Hofmann F, Biel M (1999) Two pacemaker channels from human heart with profoundly different activation kinetics. EMBO J 18:2323–2329.

Ludwig A, Budde T, Stieber J, Moosmang S, Wahl C, Holthoff K, Langebartels A, Wotjak C, Munsch T, Zong X, Feil S, Feil R, Lancel M, Chien KR, Konnerth A, Pape HC, Biel M, Hofmann F (2003) Absence epilepsy and sinus dysrhythmia in mice lacking the pacemaker channel HCN2. EMBO J 22:216–224.

Magee JC (1998) Dendritic hyperpolarization-activated currents modify the integrative properties of hippocampal CA1 pyramidal neurons. J Neurosci 18:7613–7624.

Moons L, D'Hondt E, Pijcke K, Vandesande F (1995) Noradrenergic system in the chicken brain: Immunocytochemical study with antibodies to noradrenaline and dopamine-beta-hydroxylase. J Comp Neurol 360:331–348.

Moosmang S, Stieber J, Zong X, Biel M, Hofmann F, Ludwig A (2001) Cellular expression and functional characterization of four hyperpolarization-activated pacemaker channels in cardiac and neuronal tissues. Eur J Biochem 268:1646–1652.

Mulders WH, Robertson D (2001) Origin of the noradrenergic innervation of the superior olivary complex in the rat. J Chem Neuroanat 21:313–322.

Notomi T, Shigemoto R (2004) Immunohistochemical localization of I_h channel subunits, HCN1–4, in the rat brain. J Comp Neurol 471:241–276.

Pape HC (1996) Queer current and pacemaker: the hyperpolarization-activated cation current in neurons. Annu Rev Physiol 58:299–327.

Rall W (1969) Time constants and electrotonic length of membrane cylinders and neurons. Biophys J 9:1483–1508.

Rathouz M, Trussell LO (1998) Characterization of outward currents in neurons of the avian nucleus magnocellularis. J Neurophysiol 80:2824–2835.

Reyes AD, Rubel EW, Spain WJ (1996) *In vitro* analysis of optimal stimuli for phase-locking and time-delayed modulation of firing in avian nucleus laminaris neurons. J Neurosci 16:993–1007.

Robinson RB, Siegelbaum SA (2003) Hyperpolarization-activated cation currents: from molecules to physiological function. Annu Rev Physiol 65:453–480.

Rubel EW, Parks TN (1975) Organization and development of the brain stem auditory nuclei of the chicken: tonotopic organization of n. magnocellularis and n. laminaris. J Comp Neurol 164:411–434.

Santoro B, Tibbs GR (1999) The HCN gene family: molecular basis of the hyperpolarization-activated pacemaker channels. Ann NY Acad Sci 868:741–764.

Santoro B, Liu DT, Yao H, Bartsch D, Kandel ER, Siegelbaum SA, Tibbs GR (1998) Identification of a gene encoding a hyperpolarization-activated pacemaker channel of brain. Cell 93:717–729.

Santoro B, Chen S, Lüthi A, Pavlidis P, Shumyatsky GP, Tibbs GR, Siegelbaum SA (2000) Molecular and functional heterogeneity of hyperpolarization-activated pacemaker channels in the mouse CNS. J Neurosci 20:5264–5275.

Seifert R, Scholten A, Gauss R, Mincheva A, Lichter P, Kaupp UB (1999) Molecular characterization of a slowly gating human hyperpolarization-activated channel predominantly expressed in thalamus, heart, and testis. Proc Natl Acad Sci USA 96:9391–9396.

Smith DJ, Rubel EW (1979) Organization and development of brain stem auditory nuclei of the chicken: dendritic gradient in nucleus laminaris. J Comp Neurol 186:213–240.

Solomon JS, Nerbonne JM (1993) Two kinetically distinct components of hyperpolarization-activated current in rat superior colliculus-projecting neurons. J Physiol (Lond) 469:291–313.

Wynne B, Robertson D (1996) Localization of dopamine-beta-hydroxylase-like immunoreactivity in the superior olivary complex of the rat. Audiol Neurootol 1:54–64.